PHYSICAL REVIEW A VOLUME 40, NUMBER 9 NOVEMBER 1, 1989

Theory and observation of optical guiding in a free-electron laser

A. Bhattacharjee, S. Y. Cai, S. P. Chang, J. W. Dodd,
A. Fruchtman,* and T. C. Marshall
Department of Applied Physics, Columbia University, New York, New York 10027
(Received 5 June 1989)

Optical guiding in a Raman free-electron laser (FEL) is studied theoretically and experimentally. Two complimentary theoretical approaches to the problem of optical guiding in a waveguide containing a filamentary electron beam are given and shown to be in good agreement with each other in the exponential gain regime. Evidence for optical guiding of 2-mm-wavelength radiation along the electron beam in the Columbia University FEL is obtained experimentally by analysis of spatial "ring-down" data of the optical wave profile and compared with numerical simulations. These data are presented for the exponential gain regime. A similar experiment at signal saturation conditions shows a much less well-defined ring-down. We give plausible experimental as well as theoretical arguments why the ring-down pattern is less well defined. Based on the observations presented in this paper, it is not possible to validate optical guiding at saturation.

I. INTRODUCTION

In a free-electron laser (FEL), the electron beam is not only the source of energy for the radiation field, but can, in addition, distort the wave front and alter the phase velocity of the radiation. The modified index of refraction can then cause the optical beam to propagate almost self-similarly along the electron beam despite the presence of arbitrarily strong diffraction. This effect, known as optical guiding,[1-4] has been the subject of considerable theoretical research recently.[5-13] Two qualitatively different mechanisms for guiding have been elucidated in the literature.[14] The first one is gain guiding, in which loss of optical power by diffraction is compensated for by the amplification of the radiation. In order that gain guiding may dominate, a necessary condition is that the gain length be shorter than or comparable to the Rayleigh range for the radiation. The second mechanism, and more subtle than the first, is refractive guiding which can occur even if the gain length is larger than the Rayleigh range. The occurrence of refractive guiding involves the phase shift of the radiation. In the linear regime, the real and imaginary parts of the refractive index (n) characterizing the electron beam[1,2,15,16] can, under certain conditions, satisfy the relation $\mathrm{Re}n > 1$ due to the phase shift even when the gain, proportional to $\mathrm{Im}n$, is negligible. When refractive guiding dominates, the self-similarity of the optical beam results from the interference of refracted wave fronts which compensate exactly for diffractive losses. Since refractive guiding does not rely on the presence of intrinsic gain, it can occur at saturation, which can be beneficial for the performance of long, "tapered" FEL's.

There have been a few experimental observations of optical guiding. The experiment at Los Alamos National Laboratory[17] has shown a "bending" effect of the radiation contained in the optical resonator. Optical guiding influenced by gain guiding effects has been observed in the Stanford University FEL.[18] The MIT experiment,[19] originally interpreted as evidence of optical guiding, is now understood to be wave-profile modification induced by electrostatic effects. For a valuable commentary on the Stanford and MIT experiments, the reader is referred to Ref. 20.

Experimental evidence of optical guiding obtained from the Raman FEL at Columbia has been reported recently.[21] The experiment is done in a highly overmoded waveguide, and optical guiding is detected by measuring the spatial "ring-down" of the amplified radiation at a point downstream from the termination of the electron beam, using a waveguide probe. The measurements show that optical guiding occurs in the regime of exponential growth, under circumstances for which the Rayleigh range (~ 2.5 cm) is considerably shorter than the e-folding distance of power growth (~ 10 cm). The ring-down data at saturation are much less well defined, and we therefore make no claim on the validity of optical guiding at saturation based on those data. Apart from the spatial ring-down data, there is independent experimental evidence for refractive optical guiding in the Columbia experiment based upon observations of the FEL sidebands. The latter is described in detail in a companion paper,[22] and will not be repeated here, except for the remark that the diagnostic for the guiding involves only the specturm of the FEL radiation and is therefore entirely nonperturbing. In this paper, we amplify on our earlier work,[21] and correct a flaw, pointed out by Fruchtman,[23] in our numerical work[9] which neglected the effect of TM modes. (Fortunately, this effect does not alter qualitatively our earlier interpretation and conclusions.[21]) Our present numerical results, obtained by expanding the optically guided waves in a complete set of vacuum waveguide modes, is shown to be in agreement with Fruchtman's analysis in the exponential gain regime.

We now give a plan of this paper. In Sec. II, we describe the experimental setup. In Sec. II we formulate

TABLE I. Free-electron laser parameters.

Undulator period (helical)	1.7 cm
Undulator length	60 cm
Electron-beam energy	800 kV
Electron-beam pulse length	150 nsec
Beam current density	1–2 kA/cm^2
Electron-beam diameter	4 mm
Drift-tube (waveguide) diameter	18 mm
Effective "wiggler parameter" ($eB_w/k_w mc^2$)	0.2–0.4
FEL wavelength	1.9 mm

the nonlinear FEL equations required to study optical guiding in a waveguide environment by representing the optical wave in a complete set of TE and TM modes. These equations are used to simulate numerically the Columbia University experiment. In Sec. IV, we describe Fruchtman's linear fluid theory applied to the Columbia University experiment, and demonstrate agreement of this calculation with the numerical results from the formulation described in Sec. III. In Sec. V we present experimental results together with simulation results both in the exponential gain regime and at saturation. We conclude in Sec. VI with a summary and a discussion of the implications of our results.

II. EXPERIMENTAL SETUP

A schematic of the experimental apparatus is shown in Fig. 1 and a set of typical parameters which characterized the FEL performance and geometry is given in Table I. The diode, accelerator, and electron-beam diagnostics have been described elsewhere.[24] Because of the 2-mm wavelength, the FEL operates as a traveling-wave amplifier of noise which is present at its input. This results in a statistical variation of the output power, requiring the averaging of many shots taken under nearly identical accelerator conditions. To preserve the axisymmetry of the beam termination in the large waveguide, the beam strikes a polyethylene "witness plate" which permits approximately 80% of the incident radiation to pass through to the detector. This radiaiton is no longer optically guided, but its pattern of downstream interference is uniquely determined by the boundary condition at the beam termination. Figure 1 shows the setup where the spatial pattern of power in the waveguide following the termination of the electron beam is examined using a small "waveguide probe." This probe consists of a dielectric needle horn inserted into a 2-mm-diam cylindrical waveguide which transports the radiation to a Schottky-barrier detector which is sensitive to short-wavelength radiation transmitted through a mesh filter. The waveguide probe is sensitive to radiation in a narrow forward-directed lobe of half-width 10°. The electromagnetic (EM) fields induce a wave on the dielectric element, which itself couples radiation into the miniature waveguide. The design is such that radial resolution (~ 1 mm) is purchased at the expense of axial resolution (~ 1 cm). On the other hand, we also will report measurements of the total power output of the FEL, in which case the waveguide probe is removed from the pipe and the detector is placed downstream well beyond the vacuum window of the FEL. The FEL does not oscillate because of the polyethylene plug and the absence of a high reflectivity surface at the end of the FEL. The position of the plug can be varied along the axis of the undulator. The experiment uses a constant magnetic field (1 T) for guiding and focussing of the electron beam; this magnetic field has almost no effect on the FEL other than to enhance the quiver motion of the electrons that is driven by the helical undulator "pump" field. The undulator is designed with an adiabatic entry and exit zone of a slowly varying pump field $\mathbf{B}_\perp$. The "effective" pump strength parameter is defined as $a_w = |\gamma \mathbf{v}_\perp / c|$, where $\mathbf{v}_\perp$ is the actual electron quiver velocity due to the undulator.

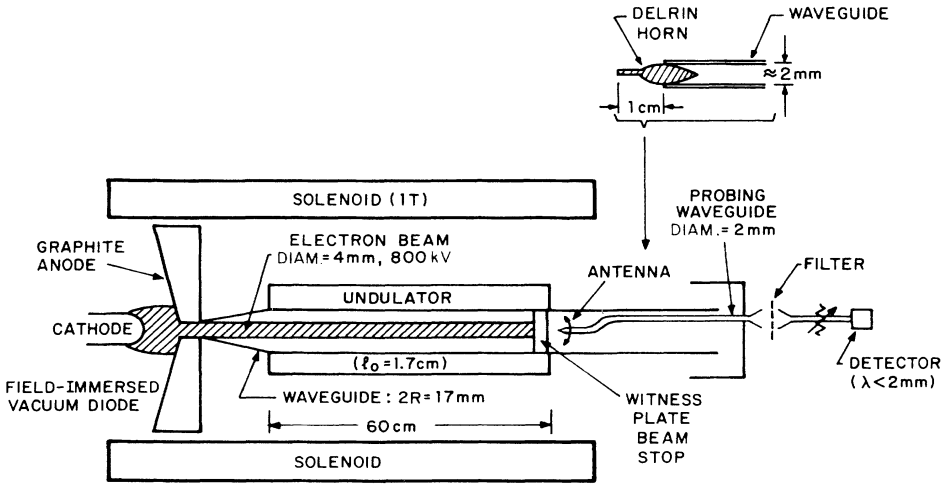

FIG. 1. Schematic of the experimental apparatus.

III. FORMULATION OF NONLINEAR EQUATIONS IN A WAVEGUIDE

The linear regime and the dispersion equation for a FEL in a waveguide has been studied exhaustively by numerous authors.[25,26] Our goal here is to develop a set of nonlinear equations for an overmoded waveguide which can be used to follow the time-evolution of the electrons and the radiation field from noise to saturation. From Maxwell's equations,

$$\nabla\times\mathbf{E}=-\frac{1}{c}\frac{\partial\mathbf{B}}{\partial t}\ , \tag{1}$$

$$\nabla\times\mathbf{B}=\frac{4\pi}{c}\mathbf{J}+\frac{1}{c}\frac{\partial\mathbf{E}}{\partial t}\ , \tag{2}$$

$$\nabla\cdot\mathbf{E}=4\pi p\ , \tag{3}$$

$$\nabla\cdot\mathbf{B}=0\ , \tag{4}$$

where $\mathbf{E}$ is the electric field, $\mathbf{B}$ the magnetic field, ρ the charge density, and $\mathbf{J}$ the current density, we get the wave equations,

$$\nabla^2\mathbf{E}-\frac{1}{c^2}\frac{\partial^2\mathbf{E}}{\partial t^2}=4\pi\nabla\rho+\frac{4\pi}{c^2}\frac{\partial\mathbf{J}}{\partial t}\ , \tag{5}$$

$$\nabla^2\mathbf{B}-\frac{1}{c^2}\frac{\partial^2\mathbf{B}}{\partial t^2}=-\frac{4\pi}{c}\nabla\times\mathbf{J}\ . \tag{6}$$

For a cylindrical waveguide with its axis in the z direction which is also the direction of wave propagation, it is sufficient to determine E_z and B_z from which the other components of $\mathbf{E}$ and $\mathbf{B}$ can be calculated. We therefore consider the z components of Eqs. (5) and (6), given by

$$\left[\nabla^2-\frac{1}{c^2}\frac{\partial^2}{\partial t^2}\right]E_z=\frac{4\pi}{c}\nabla_\perp\cdot\mathbf{J}_\perp\ , \tag{7}$$

and

$$\left[\nabla^2-\frac{1}{c^2}\frac{\partial^2}{\partial t^2}\right]B_z=-\frac{4\pi}{c}(\nabla\times\mathbf{J})_z\ , \tag{8}$$

where $\mathbf{J}_\perp$ is the transverse current produced by electron motion. The FEL has a circularly polarized undulator, specified by a vector potential,

$$\mathbf{A}_W=-\frac{mc^2}{e}a_w[\mathbf{x}\cos(\int_0^z k_w(z')dz') +\mathbf{y}\sin(\int_0^z k_w(z')dz')]\ , \tag{9}$$

where m and $-e$ are the rest mass and charge of an electron, respectively, a_w is the normalized vector potential, and $k_w=2\pi/\lambda_w$ is the wave number of the undulator. We take a_w and k_w to be given functions of z, neglecting transverse variations of the undulator field since the electron-beam radius is much smaller than the undulator period. The equations of motion for the electron are given by

$$\frac{d\gamma_j}{dz}=\frac{-k_s a_w a_s}{\gamma_j}\sin\psi_j +\frac{2\omega_p^2}{k_s c^2}(\langle\cos\psi\rangle\sin\psi_j-\langle\sin\psi\rangle\cos\psi_j)\ , \tag{10}$$

$$\frac{d\psi_j}{dz}=k_w+k_s-k_s\left[1-\frac{1+a_w^2-2a_s a_w\cos\psi_j}{\gamma_j^2}\right]^{-1/2} +\frac{\partial\phi}{\partial z}\ . \tag{11}$$

Here z is used as the independent variable, γ_j is the relativistic mass factor of the jth electron; $\psi_j=\int_0^{z_j}(k_s+k_w)dz'-\omega t+\varphi$ is the phase of the jth electron with respect to the radiation field; φ is the phase shift of the radiation field; $k_s=\omega/c$ is the wave number of the signal wave and ω, is the frequency; a_s is the normalized vector potential for the signal wave; n_0 is the electron density, assumed to be uniform at $z=0$, and $\omega_p=(4\pi n_0 e^2/m)^{1/2}$ is the plasma frequency of the beam. The angular brackets indicate an ensemble average over all electrons.

We expand E_z and B_z in a complete set of vacuum TE and TM waveguide modes,

$$E_z=\frac{mc^2}{e}\sum_{l,m}a_{lm}(z)J_l(\nu_{lm}r)\exp(il\theta) \times\exp[i(k_{lm}z-\omega t)]\ , \tag{12}$$

$$B_z=-\frac{imc^2}{e}\sum_{l,m}\frac{k_{lm}}{k_s}c_{lm}(z)J_l(K_{lm}r)\exp(il\theta) \times\exp[i(k_{lm}z-\omega t)]\ , \tag{13}$$

where J_l is the Bessel function of order l and k_{lm}, K_{lm}, q_{lm}, and ν_{lm} are determined by the boundary conditions $(d/dr)[J_l(K_{lm}r)]|_{r=R}=0$, $J_l(\nu_{lm}R)=0$. Here R is the radius of the waveguide, and $K_{lm}^2+k_{lm}^2=\nu_{lm}^2+q_{lm}^2=\omega^2/c^2$. We assume that the amplitudes $a_{lm}(z)$ and $c_{lm}(z)$ are slowly varying functions of z and neglect terms containing their second derivatives. From Eqs. (7) and (8), we get

$$\sum_{l,m}2iq_{lm}\frac{da_{lm}}{dz}J_l(\upsilon_{lm}r)\exp[i(l\theta+q_{lm}z)] =\frac{\omega_p^2 a_w}{c^2}\exp[i(\theta+k_s z)]\left[\frac{\partial}{\partial r}A-A\delta(r-r_b)\right]\ , \tag{14}$$

and

$$\sum_{l,m}2i\frac{k_{lm}^2}{k_s}\frac{dc_{lm}}{dz}J_l(K_{lm}r)\exp[i(l\theta+k_{lm}z)] =\frac{\omega_p^2 a_w}{c^2}\exp[i(\theta+k_s z)]\left[\frac{\partial}{\partial r}A-A\delta(r-r_b)\right]\ , \tag{15}$$

where r_b is the radius of the electron beam and $A=\langle\exp[-i(\psi_j-\varphi)]/\gamma_j\rangle$. We now assume that the quantity A is independent θ and neglect any poloidal

asymmetry of the beam, which implies that the only surviving terms in Eq. (14) and (15) are those with $l=1$. We let $a_{lm}(z)=a_m(z)\delta_{l,1}$ and $c_{lm}(z)=c_m(z)\delta_{l,1}$ and drop all subscripts l. We finally obtain

$$\frac{da_m}{dz}=\frac{ia_w\omega_p^2}{c^2}\frac{\nu_m}{q_m}\frac{\exp[i(k_s-q_m)z]}{R^2J_1'^2(\nu_m R)}\int_0^{r_b}dr\,rJ_0(\nu_m r)A\ , \tag{16}$$

and

$$\frac{dc_m}{dz}=\frac{ia_w\omega_p^2}{c^2}\frac{k_sK_m}{k_m^2}\frac{\exp[i(k_s-k_m)z]}{(R^2-K_m^{-2})J_1^2(K_mR)}\times\int_0^{r_b}dr\,rJ_0(K_mR)A\ . \tag{17}$$

The final step required to complete the FEL equations is to relate the quantities a_s and ϕ in Eq. (10) and (11) with the waveguide modes. This is done by using the relations $\mathbf{B}=\nabla\times\mathbf{A}$ and $\mathbf{E}=-(1/c)(\partial\mathbf{A}/\partial t)$. The vector potential associated with the signal is taken in the left-circularly-polarized form,

$$\mathbf{A}_s=\frac{mc^2}{e}a_s(\mathbf{r},t)[\hat{\mathbf{x}}\cos(k_sz-\omega t+\phi)-\hat{\mathbf{y}}\sin(k_sz-\omega t+\phi)]\ . \tag{18}$$

We then find that

$$u(\mathbf{r},t)\equiv a_se^{i\phi}=\frac{1}{2k_s}\sum_m\left[c_m\frac{k_m}{K_m}J_0(K_mr)e^{i(k_m-k_s)z}+a_m\frac{q_m}{\nu_m}J_0(\nu_mr)e^{i(q_m-k_s)z}\right]\ . \tag{19}$$

Equations (10), (11), (16), (17), and (19), which comprise a complete set, are integrated numerically to describe two-dimensional (2D) dynamics in a waveguide, both in the exponential gain regime and at saturation. As stated in Sec. II, the experiment uses a constant axial field for guiding and focusing the electron beam, which has almost no effect on the FEL other than to enhance the quiver motion of the electrons that is driven by the helical undulator field. This motion is included in the numerical calculation of the quiver velocity $(\mathbf{v}_\perp/c)_{\rm rms}$ in the undulator.

The results of the numerical simulation will be presented with the experimental results in Sec. IV. In the next section, we describe an analytical eigenmode calculation, which is valid in the exponential gain regime and provides an independent benchmark for the numerical simulation.

IV. LINEAR EIGENMODE ANALYSIS

The transverse profile of the electromagnetic wave propagating self-similarly in a FEL can be obtained by a linear analysis of the cold-fluid equations for electrons coupled with the self-consistent Maxwell's equations. In this analysis, it is possible to solve for the actual eigenmodes (and eigenvalues) of the system without the use of vacuum modes or of other systems of orthogonal functions. The analysis clarifies the roles of the FEL interaction and boundary conditions in the coupling of TE and TM sets of modes, and provides an independent check for the predictions of the 2D computer code. The details of the formalism, with and without a waveguide, are described elsewhere.[23] Here we briefly review the analysis in the presence of a waveguide. The starting point of the analysis is the cold-fluid equations for the electrons, given by the continuity equation,

$$\frac{1}{c}\frac{\partial}{\partial t}(h\gamma)+\nabla\cdot(h\mathbf{P})=0\ , \tag{20}$$

and the momentum equation,

$$\frac{\gamma}{c}\frac{\partial\mathbf{P}}{\partial t}+\mathbf{P}\cdot\nabla P=-(\gamma\mathbf{E}'+\mathbf{P}\times\mathbf{B}')\ ; \tag{21}$$

here $\mathbf{P}\equiv\gamma\mathbf{v}/c$, $\mathbf{v}$ is the electron velocity, $\mathbf{E}'=(e/mc^2)\mathbf{E}$, $\mathbf{B}'=(e/mc^2)\mathbf{B}$, $\gamma^2=1+\mathbf{P}\cdot\mathbf{P}$, and $h\equiv\omega_p^2/c^2\gamma$ is the normalized fluid density. For simplicity, we consider an untapered helical wiggler with the magnetic field,

$$\mathbf{B}_w=B_w(\hat{\mathbf{r}}\cos\Phi-\hat{\boldsymbol{\theta}}\sin\Phi)\ , \tag{22}$$

where (r,θ,z) represents the standard cylindrical coordinate system, and $\Phi=\theta-k_wz$. We assume that the beam is thin, i.e., $k_wr_b\ll1$, and that the equilibrium flow is given by

$$\mathbf{P}=-a_w(\hat{\mathbf{r}}\cos\Phi-\hat{\boldsymbol{\theta}}\sin\Phi)+(\gamma^2-1-a_w^2)^{1/2}\hat{\mathbf{z}}\ . \tag{23}$$

We linearize Eqs. (20) and (21), assuming the $P_\perp\ll P_z$, and that the perturbed quantities vary much more rapidly along the axis than along the transverse directions. Any perturbed quantity δg is represented as

$$\delta g(r,\Phi,z,t)=\sum_{n=-\infty}^{+\infty}\delta g^{(n)}(r)\exp[i(n\Phi+qz-\omega t)]\ , \tag{24}$$

where

$$\frac{\partial}{\partial z}=\frac{\partial}{\partial z}-k_w\frac{\partial}{\partial\Phi}\ , \tag{25a}$$

$$\frac{\partial}{\partial\theta}=\frac{\partial}{\partial\Phi}\ , \tag{25b}$$

and we define

$$k_z=q-lk_w\ . \tag{25c}$$

We now limit ourselves to the case in which one helical harmonic, say $n=l$, is dominant. In this case $\delta\mathbf{E}_\perp'^{(l)}$ and $\delta\mathbf{B}_\perp'^{(l)}$ are dominant, and are coupled to $\delta h^{(l-1)}$, $\delta P_z^{(l-1)}$, and $\delta E_z'^{(l-1)}$. The continuity equation for $\delta h^{(l-1)}$ becomes

$$[-\gamma\omega/c+(k_z+k_w)P_z]\delta h^{(l-1)}\simeq h[P_z\omega/(\gamma c)-(k_z+k_w)]\delta P_z^{(l-1)}\ . \tag{26}$$

The momentum equation for $\delta P_z^{(l-1)}$ becomes

$$i[-\gamma\omega/c+(k_z+k_w)P_z]\delta P_z^{(l-1)} = -\gamma\delta E_z'^{(l-1)}+(ck_z/\omega)a_w\delta E_+'^{(l)} , \quad (27)$$

where

$$\delta E_\pm' \equiv \frac{\delta E_r' \mp i\delta E_\theta'}{2} . \quad (28)$$

We now turn to Maxwell's equations (1)–(4) in which

$$\rho' \equiv 4\pi\rho = -h\gamma \quad (29)$$

and

$$\mathbf{J}' \equiv \frac{4\pi}{c}\mathbf{J} = -h\mathbf{P} . \quad (30)$$

After linearization, Eq. (3) gives

$$i(k_z+k_w)\delta E_z'^{(l-1)} = -\gamma\delta h^{(l-1)} - \frac{hP_z}{\gamma}\delta P_z^{(l-1)} . \quad (31)$$

Equations (26), (27), and (31) are algebraic equations for $\delta h^{(l-1)}$, $\delta P_z^{(l-1)}$, and $\delta E_z'^{(l-1)}$. The lth harmonic of the perturbed transverse current is obtianed from the relation

$$i\delta J_r'^{(l)} = \delta J_\theta'^{(l)} \simeq -Q\delta E_+'^{(l)} . \quad (32)$$

where

$$Q \equiv \frac{ha_w^2(k_z+k_w-\omega P_z/\gamma c)}{2\{[(k_z+k_w)P_z-\gamma\omega/c]^2-h(1+a_w^2)\}} . \quad (33)$$

Thus, the expressions for $\delta J_\perp'^{(l)}$ are as if the system is one dimensional. The transverse dependence, however, appears in $\delta\rho^{(l)}$ and $\delta J_z^{(l)}$. From the lth harmonic of Eq. (20), and the longitudinal component of Eq. (21), it can be shown that[23]

$$\delta\rho'^{(l)} \simeq -\frac{\gamma}{k_z P_z-\gamma\omega/c}\left[\frac{\partial}{\partial r}-\frac{l-1}{r}\right](Q\delta E_+'^{(l)}) , \quad (34)$$

and

$$\delta J_z'^{(l)} \simeq -\frac{P_z}{k_z p_z-\gamma\omega/c}\left[\frac{\partial}{\partial r}-\frac{(l-1)}{r}\right](Q\delta E_+'^{(l)}) . \quad (35)$$

From the transverse components of Eq. (5), we obtain

$$\frac{1}{r}\frac{\partial}{\partial r}\left[r\frac{\partial\delta E_+'^{(l)}}{\partial r}\right] + \left[\frac{\omega^2}{c^2}-k_z^2-\frac{(l-1)^2}{r^2}-\frac{\omega}{c}Q\right]\delta E_+'^{(l)}=0 , \quad (36)$$

and

$$\frac{1}{r}\frac{\partial}{\partial r}\left[r\frac{\partial\delta E_-'^{(l)}}{\partial r}\right] + \left[\frac{\omega^2}{c^2}-k_z^2-\frac{(l+1)^2}{r^2}\right]\delta E_-'^{(l)}=0 . \quad (37)$$

After further simplification, Eqs. (36) and (37) reduce to

$$\left[\frac{\partial^2}{\partial r^2}+\frac{1}{r}\frac{\partial}{\partial r}-\frac{l^2}{r^2}+\frac{\omega^2}{c^2}-k_z^2\right](\delta B_z'^{(l)}+i\delta E_z'^{(l)})=0 \quad (38)$$

and

$$\left[\frac{\partial^2}{\partial r^2}+\frac{1}{r}\frac{\partial}{\partial r}-\frac{l^2}{r^2}+\frac{\omega^2}{c^2}-k_z^2-\frac{\omega}{c}Q\right] \times(\delta B_z'^{(l)}-i\delta E_z'^{(l)})=0 , \quad (39)$$

which are coupled by virtue of the boundary conditions,

$$\delta E_z'=0, \quad \frac{\partial}{\partial r}\delta B_z'=0 , \quad (40)$$

at $r=R$. In the vacuum limit $Q=0$, Eq. (38) and (39) reduce to the standard decoupled equation for $\delta B_z'$ and $\delta E_z'$ describing TE and TM modes. Using the conditions (40) and the jump conditions at $r=r_b$[23], we obtain the dispersion equation (for $Q\neq 0$),

$$[\pi k_\perp R J_l(k_\perp R)\dot{Y}_l(k_\perp r_b)-1][s\dot{J}_{l-1}(sr_b)J_{l-1}(k_\perp r_b)-k_\perp\dot{J}_{l-1}(k_\perp r_b)J_{l-1}(sr_b)] - \pi k_\perp R J_l(k_\perp R)\dot{J}_l(k_\perp R)[s\dot{J}_{l-1}(sr_b)Y_{l-1}(k_\perp r_b)-k_\perp\dot{Y}_{l-1}(k_\perp r_b)J_{l-1}(sr_b)]=0 , \quad (41)$$

where the overdot in Eq. (37) denotes a derivative, and

$$k_\perp^2 \equiv \omega^2/c^2-k_z^2 , \quad (42a)$$

$$s^2 \equiv k_\perp^2-(\omega/c)Q . \quad (42b)$$

Here ω is given aproximately by the formula

$$\omega = 2k_w c\gamma^2/(1+a_w^2) , \quad (43)$$

well-known from one-dimensional theory. Equation (41) can then be solved numerically to determine the eigenvalue.

We now compare the results of this analysis with predictions from the 2D computer code described in Sec. II. We take the electron-beam current to be 2 kA/cm^2, $r_b=0.2$ cm, $R=0.9$ cm, $\gamma=2.5$, and $a_w=0.3$. Equation (41) then gives, for $l=1$ and $\omega/c=32.9$ cm^{-1}, the eigenvalue for the most unstable mode to be $k_z=32.8-i0.052$ cm^{-1}. For the same set of parameters the 2D code gives $\omega/c\simeq 33.0$ cm^{-1} and a growth rate of 0.056 cm^{-1}, which is in good agreement with the imaginary part of k_z quoted earlier. It is interesting to note that if the TM modes in the 2D code are artificially "switched off" by setting $c_m=0$, the growth rate is reduced slightly to 0.052 cm^{-1}. Thus, for typical operating parameters of the Columbia University FEL, the neglect of TM-mode coupling does not have a large effect on the growth rate of the FEL eigenmode in the exponential gain regime. The effect of TM-mode coupling is more pronounced during spatial "ring-down" which we will describe in the next section.

Figure 2(a) shows $\delta E=|\delta\mathbf{E}|$ (with arbitrary normaliza-

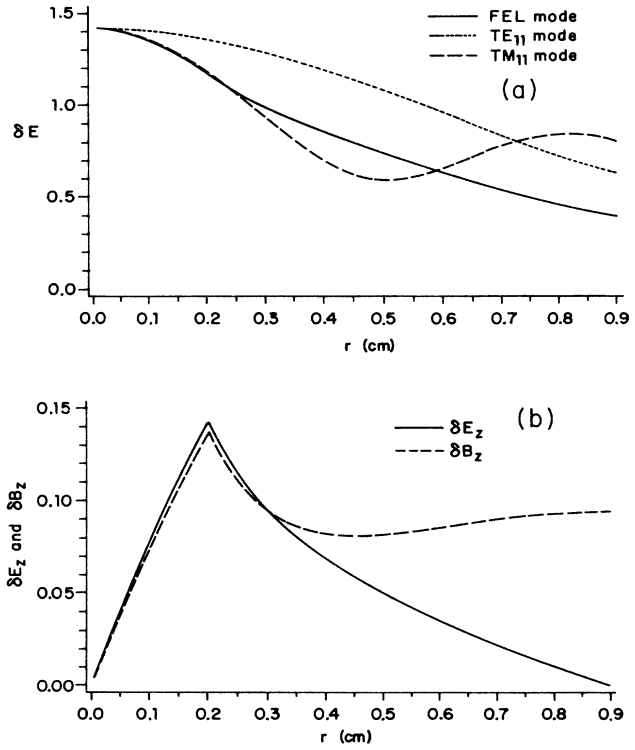

FIG. 2. (a) δE of the FEL eigenmode is compared with δE for the TE_{11} and TM_{11} vacuum modes. The FEL mode has a mixed character. (b) $|\delta E_z|$ and $|\delta B_z|$ of the FEL mode.

tion) of the FEL eigenmode as a function of r. The result of the 2D waveguide code is essentially identical with this curve. For comparison, we also show the radial profiles of δE for the TE_{11} and TM_{11} vacuum modes. Figure 2(b) shows the longitudinal wave components δE_z and δB_z of the FEL mode. We note that they are of comparable magnitude, signifying the mixed character of the eigenmode.

V. EXPERIMENTAL RESULTS AND COMPARISON WITH NUMERICAL SIMULATION

A. Linear regime of exponential growth

The experiment is first operated in the regime of exponential growth. Given the noise level of the input and the length of the undulator, we find that the interaction remains in the linear regime over most of the undulator for $a_w \leq 0.3$. Figure 3(a) shows the wave profile that results from the numerical computation of power growth and guiding along the electron beam in the overmoded waveguide for $a_w = 0.3$, with other parameters as they are in Table I. We start the simulation with zero initial radiation field and noise generated by the random distribution of electrons in phase. The wave profile shows the expected features of exponential growth and profile narrowing (which enhances the filling factor) as the wave moves down the undulator. When the electron beam is terminated by the polyethylene beam stop, the optically guided power is released from the beam and radiates in the empty drift-tube waveguide, which contains the probe. The FEL eigenmode breaks up into many vacuum eigenmodes that display a characteristic spatial interference ("ring-down"). Our experiment measures the spatial profile of the ring-down. The computed ring-down (viewed from a downstream point) is shown in Fig. 3(b).

The measurements previously reported[21] are now presented in Fig. 4, together with the prediction of theory (indicated by solid lines). The plots from theory now contain the TM as well as the TE set of modes, whereas in Ref. 21 only TE modes were retained. The computed distribution of power taken at $r = 0$ along the axis [Fig. 4(a)] shows major differences with respect to the result presented earlier [Fig. 4(a), Ref. 21], yet the fit of the data to theory is neither better nor worse than the earlier fit. Perhaps this can be anticipated in a highly overmoded system such as ours, in which the "sloshing" characteristic of the interference pattern can be reproduced approxi-

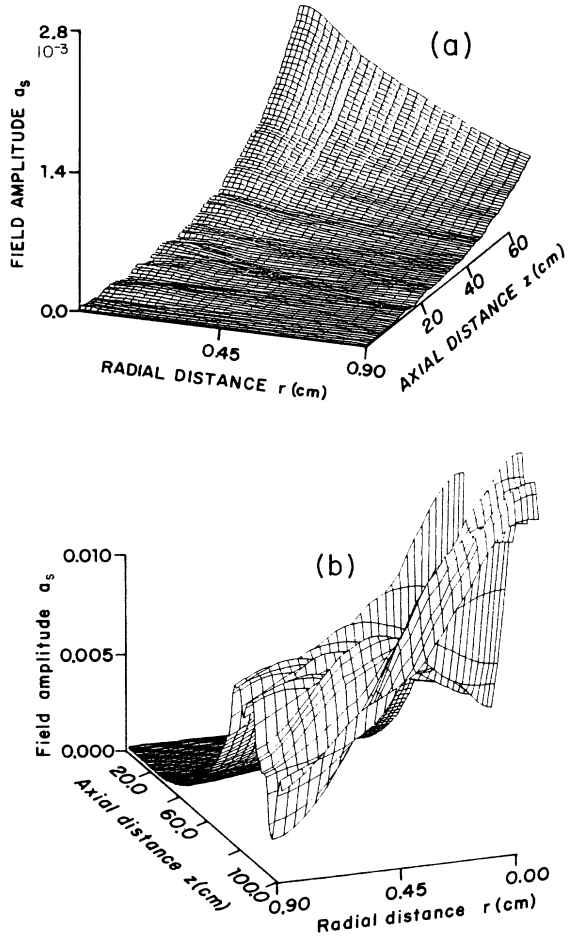

FIG. 3. (a) Wave profile in the exponential gain regime for $a_w = 0.3$, with other parameters given in Table I. (b) Computed ring-down pattern for the parameters of (a) when the electron beam is terminated at $z = 50$ cm.

mately even if a truncated set of modes are considered. Figures 4(b) and 4(c), taken at the axial power minimum and maximum, respectively, show essentially no change in the calculated radial distribution of power when compared with the corresponding curves in Ref. 21. The numerical study shows the field profile at $z=20$ cm is nearly the same as that at $z=0$. (The experimental data are the same as in Ref. 21.) By moving the beam stop and repeating the measurements, we have verified that the profile remains self-similar. The data for the radial profile [Figs. 4(b) and 4(c)] display the features expected from theory.

The theory predicts that optical guiding is weak for $a_w \leq 0.2$. It is interesting to compare Fig. 4(a), obtained by taking $a_w=0.3$, with Fig. 5, which shows the power on axis for $a_w=0.2$. The axial variation in the latter case falls within the error bars of the data, which suggests that the "sloshing" is much less pronounced than that observed in the well-guided case.

It is useful to contrast our experiment with a similar

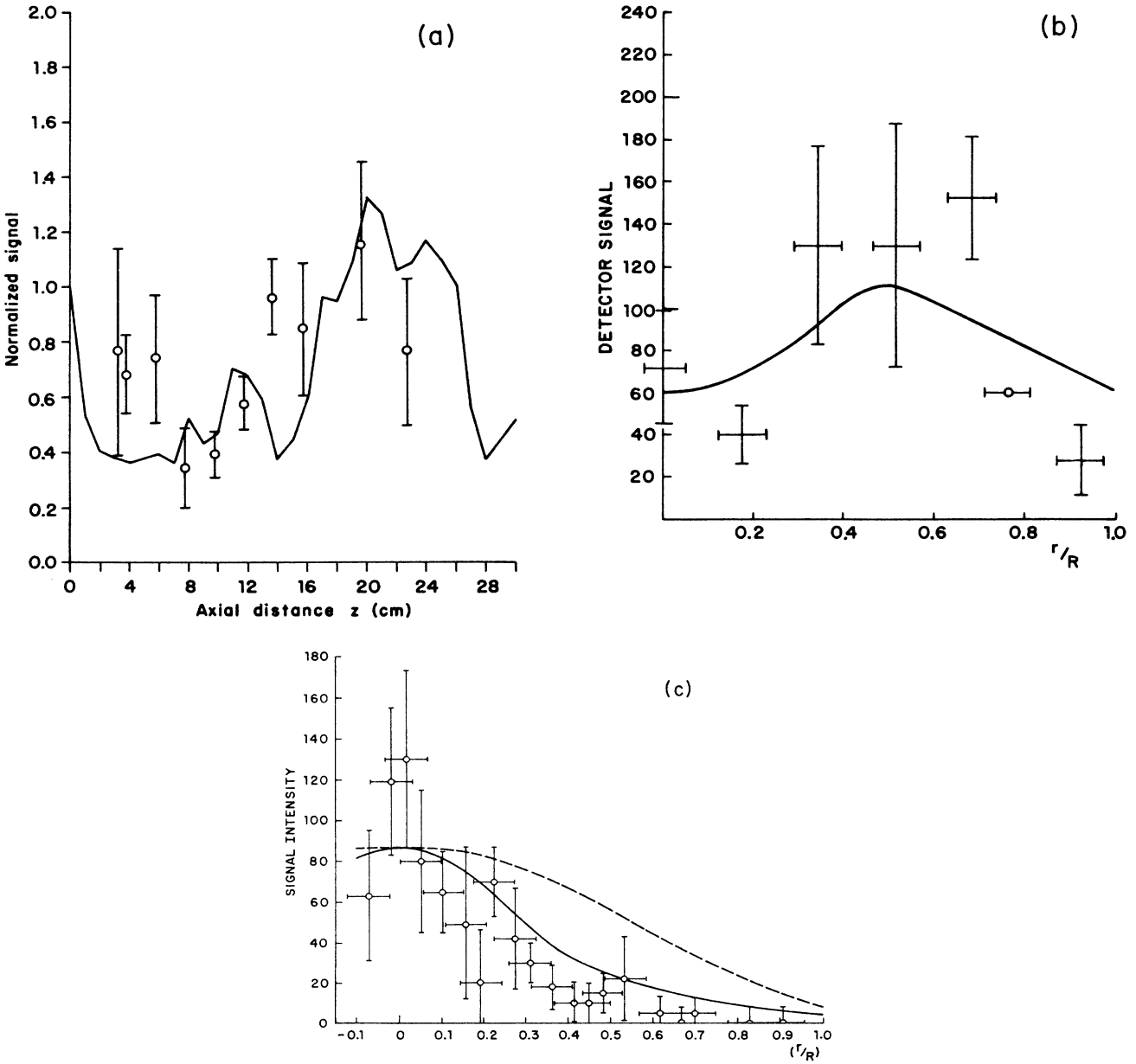

FIG. 4. (a) Experimental data (points) compared with theory (solid lines) from Fig. 3; the experimental data are the detector signal in millivolts, while the theory scale is arbitrary intensity units. This figure shows the dependence of intensity along the z axis behind the termination point ($z=50$ cm) of the electron beam. (b) Radial dependence of the intensity at $z=58$ cm. (c) Radial dependence of the intensity at $z=65$ cm. Dashed line, TE_{11} mode only; solid line, theory curve at axial maximum.

one by Masud *et al.*[26,27] using the same apparatus. A much smaller diameter (6.4 mm) waveguide was used; however, the wavelength, beam diameter, and current were nearly the same. One expects that optical guiding would be comparatively unimportant in this case. It was found that the observed growth rate agreed well with the theory given in Ref. 25 which predicts TE_{11} to be the only dominant mode in the linear regime. This could occur only if optical guiding were not important. We now compute the FEL eigenmode in accordance with the analysis in Sec. III for this case. To be specific, we take $r_b=0.2$ cm, $R=0.32$ cm, $\gamma=2.5$, $a_w=0.3$, and the current density to be 1 kA/cm^2. Equation (41) then predicts $\omega/c=28.85$ cm^{-1} and an amplitude growth rate $\simeq 0.091$cm^{-1} for the most unstable mode. In Fig. 6(a), we plot $|\delta B_z|$ and $|\delta E_z|$ for the FEL mode in this case for comparison with the guided case described by Fig. 2(b). Whereas $|\delta B_z|$ and $|\delta E_z|$ are comparable in Fig. 2(b), $|\delta E_z|$ is less than 10% of $|\delta B_z|$ in Fig. 6(a). Hence, the presence of TM modes is minimal in the composition of the FEL eigenmode in the small waveguide. As shown in Fig. 6(b), the FEL eigenmode is almost identical to the TE_{11} mode, and we confirm that optical guiding is indeed insignificant.

Since refractive guiding occurs in our experiment due to the interference of many modes, we can "switch off" the guiding effect in the computer code by decoupling artificially the waveguide modes (that is, each mode is made to interact with the electrons independently). Since this "switch" is not experimentally realizable, it is necessary to validate it by actual comparison with experimental data for a weakly guided case. This has been done in the companion paper,[22] and will not be repeated here. We compare in Fig. 7 the results of calculations for the dependence of the power growth rate upon the undulator field, with and without optical guiding. Without guiding, the growth rate increases linearly with the magnitude of the undulator field, as expected in the Raman limit. With guiding, the growth rate increases faster, particularly at higher pump field. The reason for this is that optical guiding improves the filling factor (f), which in turn enters the expression for the growth rate in 1D theory as $f^{1/2}$. Measurements of the growth rate, however, also indicated in Fig. 7, are not sufficiently accurate to fit unambiguously either curve. Thus, although the experimentally observed growth rate roughly validates the theory, the weak f dependence is experimentally difficult to verify. Nevertheless, the additional gain from optical guiding, when integrated over the length of the undulator, results

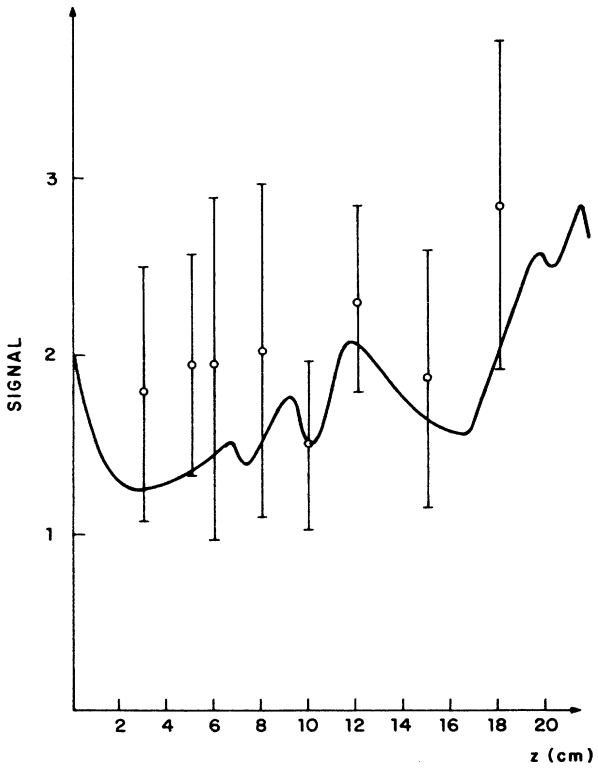

FIG. 5. Dependence of intensity along the z axis behind the termination point ($z=50$ cm) of the electron beam for the case of weak guiding ($a_w=0.2$). The axial variation falls within the error bars of the data, which suggests that the "sloshing" is much less pronounced than in the guided case [Fig. 4(a)].

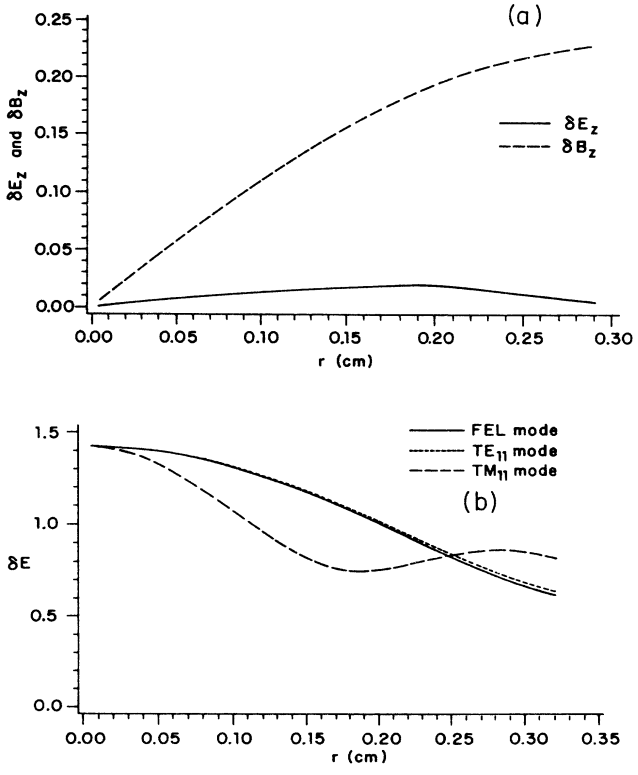

FIG. 6. (a) $|\delta E_z|$ and $|\delta B_z|$ of the FEL mode for the experiment with a smaller waveguide of radius 0.32 cm. $|\delta E_z|$ is less than 10% of $|\delta B_z|$, the FEL mode is dominantly TE_{11}, and optical guiding is insignificant. (b) δE of the FEL mode for the parameters of (a) compared with the vacuum TE_{11} and TM_{11} modes. The FEL mode is almost identical to the TE_{11} mode.

in an appreciable improvement in overall signal gain. Figure 7 shows that the most rapidly growing signal (from noise) in our experiment corresponds to the optically guided mode.

B. Saturation regime

As explained in Sec. I, refractive guiding, since it does not rely on the presence of intrinsic gain, can occur at saturation. In Ref. 22, the presence of guiding at saturation is shown to enhance somewhat the shifts of the sidebands (with respect to the carrier) as well as their growth rates, though the effect of guiding at saturation is found to be weaker than that in the exponential gain regime. Here we report on alternate experimental attempts to observe refractive guiding at saturation.

The theory predicts that when the pump field is increased to $a_w \simeq 0.4$, the amplified wave will saturate approximately two-thirds of the way down the undulator. To insure saturation on all shots, we use an undulator with a slight (and unoptimized) taper (11%) beginning half way along its total length of 70 cm; the power grows by roughly a factor of 2 along this tapered region.

Typical experimental data for the spatial ring-down following a beam stop are shown in Fig. 8. In Fig. 8, we note that the axial ring-down shows a much weaker "sloshing" behavior than that in Fig. 4(a). We give here a possible explanation as to why it may be difficult to have a conclusive demonstration of refractive guiding in the presence of a waveguide. As the signal passes into saturation, some power is lost from the optically confined, guided profile and moves out to the wall; this is illustrated by a numerical solution (Fig. 9) in which the signal saturates at $z = 50$ cm. From there, it "sloshes" to and fro in the waveguide, interfering with the electron-radiation interaction occurring near the axis. The waves reflected from the wall are generally out of phase with respect to the ponderomotive wave, and can interfere destructively with the latter, causing a local detrapping of the electrons from the ponderomotive bucket. In particular, we find that if an artifical phase shift is introduced at some point into the ponderomotive wave, an expansion of the downstream optical beam results. (Furthermore, the power released from the beam upstream also interferes

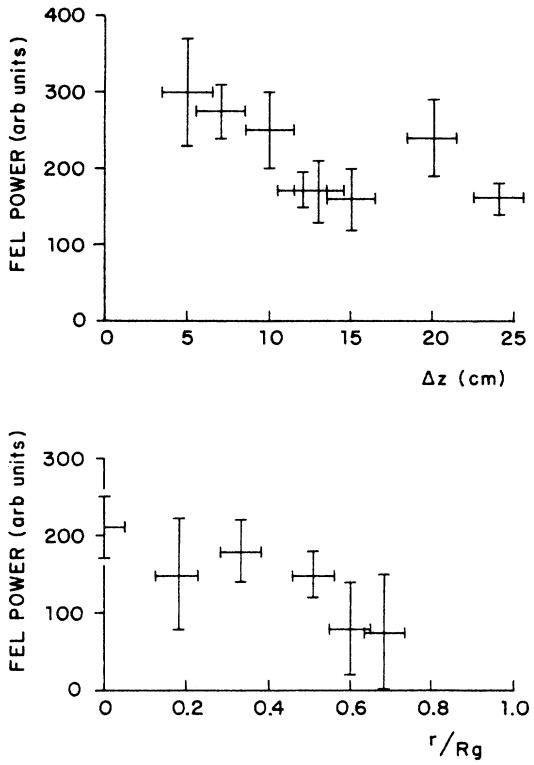

FIG. 8. Dependence of the intensity along the z axis measured from the termination point ($z = 50$ cm, $\Delta z = 0$) of the electron beam (top frame) and the radial distribution of intensity at $\Delta z = 20$ cm (bottom frame) at saturation.

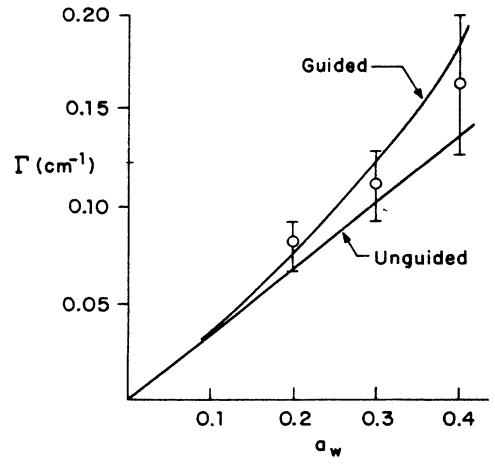

FIG. 7. Experimental data (points) of the power growth rate Γ as a function of a_w compared with theory (solid lines). The "guided" curve is calculated with modes coupled, the "unguided" curve with modes decoupled.

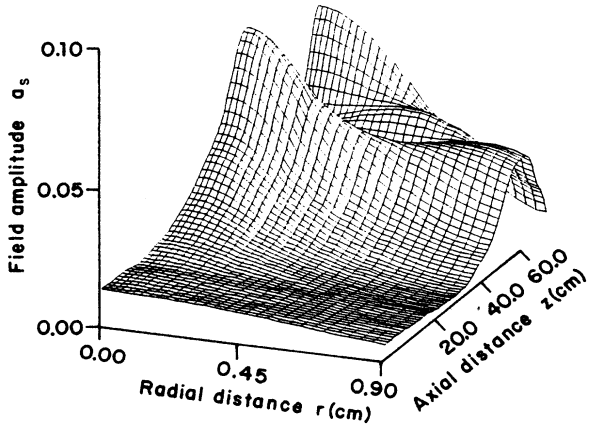

FIG. 9. Wave profile in a waveguide from start-up to saturation for $a_w = 0.3$, with other parameters given in Table I.

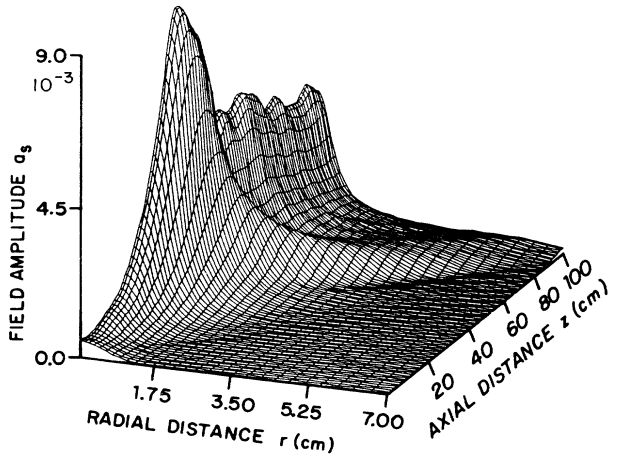

FIG. 10. Wave profile in empty space from start-up to saturation. The wave profile remains approximately self-similar at saturation.

with the radiation of the remaining guided power in the ring-down zone, resulting in a less well-defined spatial interference pattern for the experiment to detect.) On the other hand, if the experiment were done in empty space, Fig. 10 shows that though some power is lost from the beam as saturation occurs, it does not return to interfere with the FEL interaction. The profile downstream does remain approximately self-similar as it propagates, as reported by Scharlemann *et al.*[4] using shorter wavelengths. This leads us to conclude that our failure to observe optical guiding following saturation may be an artifact of the boundary conditions imposed by the waveguide geometry, and that a short-wavelength FEL experiment operating without a waveguide may find a remnant optical guiding occurring under saturation or slow growth conditions.

VI. CONCLUSION

In this and a companion paper,[22] we have attempted to validate the concept of refractive optical guiding by comparing theoretical (numerical) predictions with experimental observations in the Columbia University FEL. In the presence of a waveguide, the theory of optical guiding has certain interesting features, and we have presented in this paper two complementary methods—numerical and analytical—for the theoretical study of guiding in the exponential gain regime. We show that the two methods agree well in their predictions, and give us confidence in extending our numerical studies to the nonlinear regime.

As in Ref. 21, we believe we have presented firm, if indirect, evidence of the occurrence of optical guiding strongly influenced by refractive guiding effects in the regime of exponential gain. Refractive guiding is a subtle effect, and our approach has been to accumulate a detailed corpus of theory and experimental data, each of which adds incremental evidence in support of the concept. In the saturation regime, the experimental results presented in this paper are not conclusive, and the numerical studies suggest that the reason for this has to do with the experimental conditions, together with a weakening of the guiding effect expected from theory. (Observations of the sideband shift in the saturation regime, presented in Ref. 22, also indicate a weakening of the guiding effect.) We have given plausible arguments as to why some of the loss of guiding we observe at saturation may be attributed, somewhat paradoxically, to the presence of a waveguide. Based on these physical arguments, it is tempting to speculate that it may be possible to have a more convincing demonstration of refractive guiding in the saturation regime in a short-wavelength FEL experimental facility.

ACKNOWLEDGMENTS

This research is supported by the U. S. Office of Naval Research, Grant No. N0014-79C-0769 and the National Science Foundation, Grant No. ECS-87-13710. A. F. acknowledges the support of the Koret Foundation.

*Permanent address: Physics Department, Weizmann Institute of Science, 76100 Rehovot, Israel.

[1]N. M. Kroll, P. L. Morton, and M. N. Rosenbluth, IEEE J. Quantum Electron. **QE-17**, 1436 (1981).
[2]P. Sprangle and C. M. Tang, Appl. Phys. Lett. **39**, 677 (1981); AIAA **19**, 1164 (1981).
[3]G. T. Moore, Opt. Commun. **52**, 46 (1984).
[4]E. T. Scharlemann, A. M. Sessler, and J. M. Wurtele, Phys. Rev. Lett. **54**, 1925 (1985).
[5]G. T. Moore, Opt. Commun. **54**, 121 (1985); Nucl. Instrum. Methods Phys. Res. A **250**, 381 (1986).
[6]M. Xie and D. A. G. Deacon, Nucl. Instrum. Methods Phys. Res. A **250**, 426 (1985).
[7]P. Luchini, Nucl. Instrum. Methods Phys. Res. A **250**, 413 (1985); **259**, 150 (1986).
[8]K. J. Kim, Phys. Rev. Lett. **57**, 1871 (1986).
[9]S. Y. Cai, A. Bhattacharjee, and T. C. Marshall, IEEE J. Quantum Electron. **QE-23**, 1651 (1987).
[10]P. Sprangle, A. Ting, and C. M. Tang, Phys. Rev. Lett. **59**, 202 (1987); Phys. Rev. A **36**, 2773 (1987).
[11]S. Krinsky and L. H. Yu, Phys. Rev. A **35**, 3406 (1987).
[12]T.M. Antonsen, Jr. and B. Levush, Nucl. Instrum. Methods Phys. Res. A **272**, 472 (1988).
[13]A. Fruchtman, Phys. Rev. A **37**, 2989(1988).
[14]See, for instance, E. T. Scharlemann, Proc. SPIE **738**, 129 (1987).
[15]J. M. Slater and D. D. Lowenthal, J. Appl. Phys. **52**, 44 (1981).
[16]D. Prosnitz, A. Szoke, and V. K. Neil, Phys. Rev. A **24**, 1436 (1981).
[17]R. W. Warren and B. D. McVey, Nucl. Instrum. Methods Phys. Res. A **259**, 154 (1987).

[18]J. E. LaSala, D. A. G. Deacon, and J. M. J. Madey, Phys. Rev. Lett. **59**, 2047 (1987).
[19]F. Hartemann, K. Xu, G. Bekefi, J. S. Wurtele, and J. Fajans, Phys. Rev. Lett. **59**, 1177 (1987).
[20]E. Jerby and A. Gover, Phys. Rev. Lett. **63**, 864 (1989).
[21]A. Bhattacharjee, S. Y. Cai, S. P. Chang, J. W. Dodd, and T. C. Marshall, Phys. Rev. Lett. **60**, 1254 (1988).
[22]S. Y. Cai, A. Bhattacharjee, S. P. Chang, J. W. Dodd, and T. C. Marshall, Phys. Rev. A **40**, 3127 (1989).
[23]A. Fruchtman (unpublished).
[24]S. C. Chen and T. C. Marshall, IEEE J. Quantum Electron. **QE-21**, 924 (1985).
[25]H. P. Freund and A. K. Ganguly, Phys. Rev. A **28**, 3438 (1983).
[26]J. Masud, Ph.D. thesis, Columbia University, 1986, and references therein.
[27]J. Masud, T. C. Marshall, S. P. Schlesinger, and F. G. Yee, IEEE J. Quantum Electron **QE-23**, 1594 (1987).